ELSEVIER

Surface Science 466 (2000) L821–L826

surface science

www.elsevier.nl/locate/susc

Surface Science Letters

Electronic contrast in scanning tunneling microscopy of Sn–Pt(111) surface alloys

M. Batzill, D.E. Beck, B.E. Koel *

Department of Chemistry, University of Southern California, Los Angeles, CA 90089-0482, USA

Received 16 August 2000; accepted for publication 23 August 2000

Abstract

Scanning tunneling microscopy studies of mixed domain p(2×2) and $(\sqrt{3}\times\sqrt{3})$R30° tin–platinum surface alloys are presented. It was found that the apparent height of Pt ensembles increases with a decreasing number of Sn next-neighbor atoms per Pt atom. This is explained by a reduction of the local density of states near the Fermi level at Pt sites due to the effects of alloying of Pt with Sn. © 2000 Elsevier Science B.V. All rights reserved.

Keywords: Alloys; Low index single crystal surfaces; Platinum; Scanning tunneling microscopy; Surface electronic phenomena (work function, surface potential, surface states, etc.); Tin

Chemical contrast, i.e. the discrimination between different elements at a surface, in scanning tunneling microscopy (STM) measurements has been observed for a number of systems (e.g. PtNi [1–3], PtRh [2–4], PtCo [2,5], CuAg [6], PdCu [7], PdAg [8], PtSn [9]). Although it appears that in some systems (e.g. PtNi [2]) tip–sample interactions are crucial for the observed chemical contrast, the Tersoff–Hamann theory [10] is sufficient to explain the chemical contrast in most other systems. This model states that the contrast in STM is related to the local density of states (LDOS) near the Fermi level of the surface atoms. For the PtRh alloy, for instance, sites of Rh atoms appear more corrugated than Pt sites. Hofer et al. [3] showed that this is in agreement with the higher LDOS near the Fermi level of Rh compared with Pt. They showed that alloying of Pt and Rh increases the LDOS at Rh sites around the Fermi level even more, whereas it decreases the LDOS for Pt in the same energy range.

Even more exciting than the discrimination between different elements in alloy surfaces are the observations that elements neighboring a substitutional atom can show a different apparent height compared with the same elements in an undisturbed surface lattice. For the Pt–Rh system, Hofer et al. [3] stated that the LDOS of an Rh atom should depend on the number of next-neighbor Pt atoms. No clear change in the apparent height of individual Rh atoms could, however, be observed in this *disordered* alloy surface. Other experiments on other systems hint that neighboring atoms of a different kind can change the electronic structure and cause a change in the STM contrast.

* Corresponding author. Fax: +1-213-746-4945.
E-mail address: koel@chem1.usc.edu (B.E. Koel)

PII: S0039-6028(00)00803-7

Gilarowski and Niehus [11] have reported a subsurface IrCu alloy buried in the second layer of a Cu crystal. The underlying Ir atoms induced a contrast difference in the STM images in the Cu overlayer. This may be explained by a change in the electronic structure of the Cu layer caused by the underlying Ir atoms. Intriguing results have also been achieved for Au atoms substituting for Ni atoms in an Ni (111) single crystal surface. The Ni atoms surrounding the substitutional Au atom appear brighter in STM images compared with the 'undisturbed' Ni atoms in the surface [12]. Although, a purely topographical effect could not be excluded conclusively, a change in the LDOS at the sites of the Ni atoms induced by the neighboring Au atom may explain this observation. These results suggest that it is not only possible to distinguish between different elements at a surface, but also to discriminate between the *same* element in different environments due to changes in the electronic structure of the atoms. These changes may be observed as 'electronic' contrast in STM images.

Although a change of the atomic corrugation in STM images with the number of hetero-atoms surrounding the atom is anticipated, there has been no unambiguous evidence presented so far. In this Letter we show that Pt ensembles exhibit different apparent heights in STM images depending on the number of Sn neighbor atoms per Pt atom in Sn–Pt surface alloys. Sn–Pt(111) surface alloys are well suited for the study of electronic contrast in STM because *two* stable, *ordered* surface alloys can be formed by substitutional replacement of Pt atoms by Sn in the surface layer to create the $p(2\times2)$ and $(\sqrt{3}\times\sqrt{3})R30^\circ$ alloy structures [13,14]. By preparing a surface that shows domains of both possible ordered alloy structures, the apparent height in STM images of the Pt atoms in either domain can be compared directly. This excludes possible ambiguities concerning the state of the probing tip that would arise if the two structures were imaged independently. Furthermore, domain boundaries and defects in the surface alloy were expected to exhibit a variety of Pt atom constellations for additional comparisons.

The structural [13–16] and chemical [17–21] properties of Sn–Pt(111) surface alloys have been studied extensively. The differences between the chemical properties of clean Pt(111) and the alloy surfaces have been partly accounted for by ensemble-size effects that reduce the number of contiguous Pt atoms available for adsorption and reaction sites. However, electronic (ligand) effects can also play a decisive role in the altered chemical reactivity for surfaces with different Sn concentrations.

The experiments were performed in an ultrahigh vacuum chamber with a base pressure of 2×10^{-10} Torr. The apparatus was equipped with a reverse-view low-energy electron diffraction (LEED) optics, cylindrical mirror analyzer for Auger electron spectroscopy (AES), quadrupole mass spectrometer for residual gas analysis, ion sputtering gun for sample cleaning, leak valves and gas dosing lines, and a resistively heated Sn doser. The scanning tunneling microscope was a home built, single piezo-tube design. Electrochemically etched polycrystalline W tips were used in all experiments. Standard procedures for cleaning the Pt single crystal and preparing the Pt–Sn surface alloys were used [14,22]. The Pt(111) single crystal was cleaned by using cycles of 500 eV Ar^+-ion sputtering, annealing in 2×10^{-7} Torr oxygen to 1000 K and final annealing to 1200 K in vacuum. The cleanliness of the sample was checked by AES. Sn was deposited on the Pt(111) surface at room temperature, and the tin coverage was estimated from the Sn(430 eV)/Pt(237 eV) peak-to-peak ratio in AES. Following Sn deposition, the sample was annealed to 1000 K in order to form the desired Sn–Pt (111) surface alloy.

LEED analysis of such samples confirmed that it was possible to prepare surfaces that showed the co-existence of both the $p(2\times2)$ and $(\sqrt{3}\times\sqrt{3})R30^\circ$ surface alloy phases. Fig. 1 shows an STM image of a surface region exhibiting both ordered alloy structures. Even though we have achieved atomic resolution of clean Pt(111) surfaces with our scanning tunneling microscope, we only resolve the unit cell of the Sn–Pt alloys. The Pt ensembles in the alloy structure did not show any atomic corrugation. In agreement with results by Kuntze et al. [9] on bulk $Pt_3Sn(111)$ surfaces, the Sn atoms are depicted as depressions by STM,

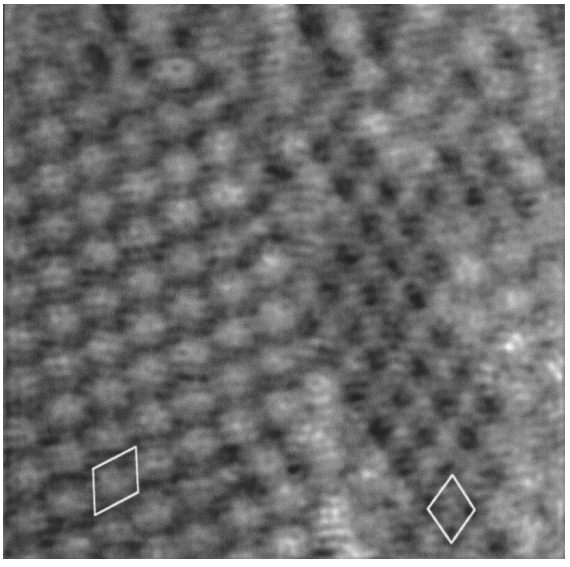

Fig. 1. STM image of p(2×2) (left) and $(\sqrt{3}\times\sqrt{3})$R30° (right) domains of an Sn–Pt (111) surface alloy. The imaged unit cells of the ordered alloys are also indicated (see also Fig. 3). Scan area: 6.3×6.3 nm^2; tunneling conditions are $U_{\text{Bias}}=2.5$ mV, $I=2$ nA.

despite the fact that they are buckled out of the surface layer by 0.022 nm [14]. This has been explained by the low LDOS near the Fermi edge at the sites of the Sn atoms compared with Pt atoms. Furthermore, the apparent height of the Pt ensembles with respect to the Sn atoms varies between the two different surface alloys. In the p(2×2) alloy, the Pt atoms appear brighter than in the $(\sqrt{3}\times\sqrt{3})$R30° alloy. Defects in the surface alloy, i.e. spots in the surface with missing Sn atoms in the alloy structure or antiphase boundaries between two $(\sqrt{3}\times\sqrt{3})$R30° domains, exhibit different apparent heights. This is shown in Fig. 2a. The apparent corrugation of these images does not change significantly with the applied bias voltage in a range between 4 and 300 mV for most tips. In one exceptional case, however, we did observe that significant contrast difference between different Pt ensembles could only be achieved for extremely low (few milllivolts) bias voltages. This may be explained by an oxidized or contaminated tip.

If the change in the apparent height is a result

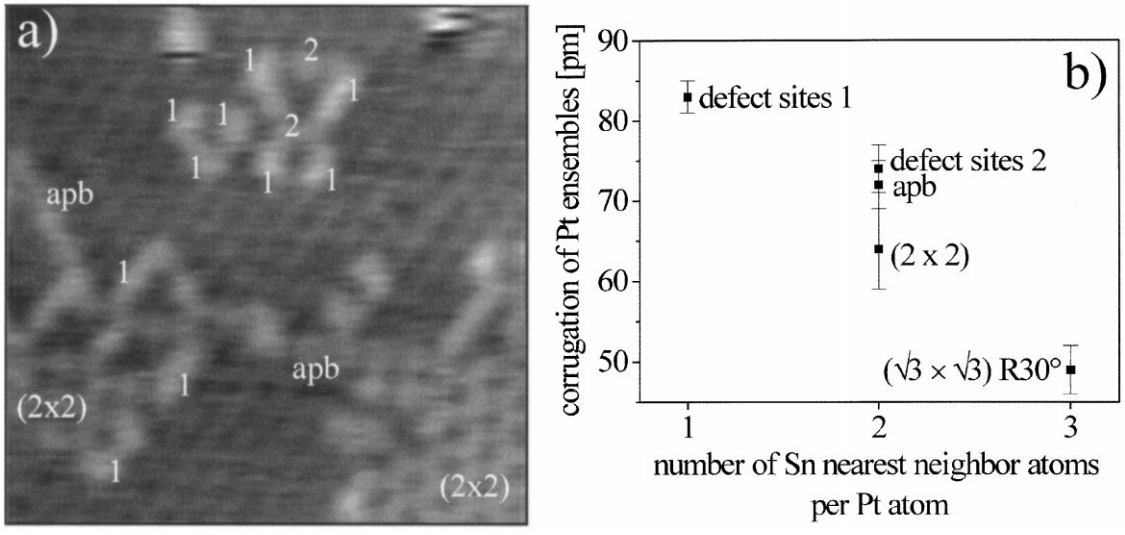

Fig. 2. (a) STM image of an Sn–Pt(111) surface alloy showing regions of both ordered alloy domains and defect sites in the alloy that are comprised of Pt ensembles with reduced Sn coordination. Antiphase boundaries (apb) in the $(\sqrt{3}\times\sqrt{3})$R30° domains are also visible. Platinum ensembles with one or two Sn neighbors per Pt atom are labeled with 1 and 2 respectively. Scan area: 7.5×7.5 nm^2; tunneling conditions: $U_{\text{Bias}}=280$ mV, $I=0.5$ nA. (b) The dependence of the corrugation of Pt ensembles measured in the STM image shown in (a) on the number of Sn neighbor atoms per Pt atom.

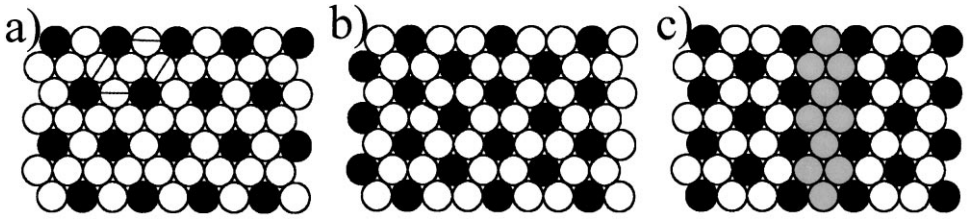

Fig. 3. Schematic illustrations of surface structures corresponding to (a) p(2×2), (b) $(\sqrt{3}\times\sqrt{3})$R30°, (c) an antiphase boundary in a $(\sqrt{3}\times\sqrt{3})$R30° alloy. Pt atoms are depicted as white and Sn atoms as black. Light gray atoms in (c) mark Pt atoms in the antiphase boundary. The unit cells in the STM images of Fig. 1 are also indicated in (a) and (b). The number of neighboring Sn atoms per Pt atom can be easily counted in these illustrations.

of alloying, then one may expect a correlation between the corrugation of the Pt ensembles in the STM images with the number of neighboring Sn atoms per Pt atom. In Fig. 3, we illustrate that every Pt atom in the $(\sqrt{3}\times\sqrt{3})$R30° alloy structure has three Sn neighbors, and that Pt atoms in the p(2×2) alloy and in an antiphase boundary have two Sn neighbors. In Fig. 2b, the corrugation of these Pt ensembles and those in defect sites with one or two Sn neighbors per Pt atom found in Fig. 2a are plotted against the number of Sn nearest neighbors per Pt atom. The tendency is for the corrugation of the Pt atoms to decrease with an increasing number of Sn neighboring atoms. Defect sites with two Sn neighbors per Pt atom, and Pt ensembles in antiphase boundaries have a slight tendency to appear brighter than Pt ensembles in the p(2×2) alloy structure that have the same number of Sn neighbors.

Topographical effects due to e.g. outward buckling of atoms can be excluded for the interpretation of the observed corrugation in the STM images. It is known from ion scattering experiments that the Sn atoms are buckled outwards by about 0.022 nm for both surface alloys [14]. Thus, we do not image directly the topographical structure of the surface. Tip–sample interactions are also unlikely to play an important role in causing the contrast for this particular system, since no significant changes could be observed with a variation in the tip–sample separation. These observations favor an electronic effect for causing the contrast in the STM images. The measured corrugation in this study of ~48 pm for the $(\sqrt{3}\times\sqrt{3})R30°$ and ~63 pm for the p(2×2) alloy (see Fig. 2b) is significantly larger than the corrugation measured, for instance, for the PtRh alloy of only 22 pm [3]. This implies a larger difference in the LDOS near the Fermi edge between Sn and Pt than between Pt and Rh.

Apart from the change in the LDOS, other effects may contribute to the observed changes in the corrugation of different platinum ensembles. The corrugation in STM images decreases exponentially with the decay length of the electronic states, which, in turn, are sensitive to the reciprocal lattice constant [10]. The shortest reciprocal lattice vector for the p(2×2) alloy is shorter than for the $(\sqrt{3}\times\sqrt{3})$R30° alloy, and thus one may expect a larger corrugation for the p(2×2) compared with the $(\sqrt{3}\times\sqrt{3})$R30° surface structure in agreement with our observations. Furthermore, differently hybridized electronic states may exhibit different decay lengths that potentially cause a change in the apparent heights in the STM images. These different electronic effects may coexist and contribute to the measured corrugation. In practice, however, it is difficult to disentangle these effects. In previous studies, only changes in the LDOS have been considered in order to explain the chemical contrast of some systems [3]. In the following we qualitatively show that such an approach can also explain our observations.

Electronic structure calculations by Pick [23] showed that hybridization between Pt-d and Sn-p electrons leads to a lowering of the LDOS at the Fermi level and a downward shift of the Pt local d-band. The Tersoff–Hamann model predicts that for negligible tip–surface interactions and a tip with s-type symmetry, the contrast in STM images

represents the LDOS of the surface around the Fermi level. Thus the difference in the apparent height of Pt atoms with different Sn-coordination in the STM images may be explained by changes of the LDOS around the Fermi level due to charge donation and rehybridization of electrons as a result of Pt–Sn alloying. Such an explanation is also in agreement with calculations by Lu et al. [24], who showed that a linear relationship between total charge transfer between an atom and the number of neighboring hetero-atoms exists for AgPd and AgAu alloys. Furthermore, they pointed out that the LDOS of a given atomic site depends not only on the number of hetero-atoms around it, but also on the distribution of the surrounding atoms. This may explain our observation that antiphase boundaries and defect sites with two Sn neighbor atoms per Pt atom show a slightly larger corrugation than Pt ensembles in the $p(2\times2)$ phase, even though the number of Sn neighboring atoms is identical. However, electronic structure calculations for Sn–Pt surface alloys will be necessary to confirm such an interpretation. Although, the arguments of Lu et al. [24] may explain the small variations in the apparent height of the Pt sites with two Sn neighbors, we cannot entirely exclude slight topographical differences at these defect sites. This is unlike the situation for the ordered alloy structures.

The different chemical reactivities of the two Sn–Pt surface alloys are also consistent with a change in the electronic structure of the Pt atoms [21]. Thus, our STM observations may be a direct probe of the chemical reactivity of certain surface sites, and also illustrates how important defects are in the overall chemical reactivity of surfaces. We should point out that the apparent height in STM images may not be directly related to the chemical reactivity in general. Although the chemical reactivity has been related to core level shifts [25] and the energy of the centroid of the metal d-band with respect to the Fermi level [26,27], STM probes mainly the LDOS around the Fermi level and so it provides only a part of the picture. In the particular case of these Pt–Sn alloys, alloying is thought to cause a depopulation of the Pt 5d band, which, in turn, can explain the reduction of the LDOS near the Fermi edge [21,23]. Consequently, the apparent height in these STM images may also be interpreted as a measure of the potential adsorption bond strength and reactivity between Pt surface atoms and adsorbed molecules.

Acknowledgements

This work was supported by the National Science Foundation (NSF) Chemistry Division. One of the authors (MB) gratefully acknowledges financial support from the Deutsche Forschungsgemeinschaft (DFG).

References

[1] M. Schmid, H. Stadler, P. Varga, Phys. Rev. Lett. 70 (1993) 1441.
[2] P. Varga, M. Schmid, Appl. Surf. Sci. 141 (1998) 287.
[3] W.A. Hofer, G. Ritz, W. Hebenstreit, M. Schmid, P. Varga, J. Redinger, R. Podloucky, Surf. Sci. 405 (1998) L514.
[4] E.L.D. Hebenstreit, W. Hebenstreit, M. Schmid, P. Varga, Surf. Sci. 441 (1999) 441.
[5] Y. Gauthier, P. Dolle, R. Baudoing-Savois, W. Hebenstreit, E. Platzgummer, M. Schmid, P. Varga, Surf. Sci. 396 (1998) 137.
[6] P.T. Sprunger, E. Lægsgaard, F. Besenbacher, Phys. Rev. B 54 (1996) 591.
[7] P.W. Murray, I. Stensgaard, E. Lægsgaard, F. Besenbacher, Surf. Sci. 365 (1996) 591.
[8] P.T. Wouda, M. Schmid, B.E. Nieuwenhuys, P. Varga, Surf. Sci. 417 (1998) 292.
[9] J. Kuntze, S. Speller, W. Heiland, A. Atrei, I. Spolveri, U. Bardi, Phys. Rev. B 58 (1998) 16 005.
[10] J. Tersoff, D.R. Hamann, Phys. Rev. B 31 (1985) 805.
[11] G. Gilarowski, H. Niehus, Surf. Sci. 436 (1999) 107.
[12] F. Besenbacher, I. Chorkendorff, B.S. Clausen, B. Hammer, A.M. Molenbroek, J.K. Nørskov, I. Stensgaard, Science 279 (1998) 1913.
[13] M.T. Paffett, R.G. Windham, Surf. Sci. 208 (1989) 34.
[14] S.H. Overbury, D.R. Mullins, M.T. Paffett, B.E. Koel, Surf. Sci. 254 (1991) 45.
[15] M. Galeotti, A. Atrei, U. Bardi, G. Rovida, M. Torrini, Surf. Sci. 313 (1994) 349.
[16] A. Atrei, U. Bardi, J.X. Wu, E. Zanazzi, G. Rovida, Surf. Sci. 290 (1993) 286.
[17] J.W. Peck, D.I. Mahon, D.E. Beck, B.E. Koel, Surf. Sci. 410 (1998) 170.
[18] M.T. Paffett, S.C. Gebhard, R.G. Windham, B.E. Koel, J. Phys. Chem. 94 (1990) 6831.

[19] C. Xu, J.W. Peck, B.E. Koel, J. Am. Chem. Soc. 115 (1993) 751.
[20] J.W. Peck, D.E. Beck, D.I. Mahon, B.E. Koel, J. Phys. Chem. B 102 (1998) 3321.
[21] J.A. Rodriguez, T. Jirsak, S. Chaturvedi, J. Hrbek, J. Am. Chem. Soc. 120 (1998) 11149.
[22] A. Atrei, U. Bardi, J.X. Wu, E. Zanazzi, G. Rovida, Surf. Sci. 290 (1993) 286.
[23] Š. Pick, Surf. Sci. 436 (1999) 220.
[24] Z.W. Lu, S.-H. Wei, A. Zunger, Phys. Rev. B 44 (1991) 10470.
[25] J.A. Rodriguez, D.W. Goodman, Science 257 (1992) 897.
[26] M. Mavrikakis, B. Hammer, J.K. Nørskov, Phys. Rev. Lett. 81 (1998) 2819.
[27] M.O. Pedersen, S. Helveg, A. Ruban, I. Stensgaard, E. Lægsgaard, J.K. Nørskov, F. Besenbacher, Surf. Sci. 426 (1999) 395.